Journal of Power Sources 195 (2010) 7462–7465

Contents lists available at ScienceDirect

Journal of Power Sources

journal homepage: www.elsevier.com/locate/jpowsour

Short communication

Liquid phase chemical synthesis of Co–S microspheres with novel structure and their electrochemical properties

Dawei Song [a], Qinghong Wang [b], Yaping Wang [b], Yijing Wang [b,*], Yan Han [b], Li Li [b], Guang Liu [b], Lifang Jiao [b], Huatang Yuan [b]

[a] School of Chemistry and Chemical Engineering, Henan University of Technology, Zhengzhou 450001, PR China
[b] Institute of New Energy Material Chemistry, Key Laboratory of Advanced Energy Materials Chemistry (MOE), Nankai University, Tianjin 300071, PR China

ARTICLE INFO

Article history:
Received 9 October 2009
Received in revised form 29 May 2010
Accepted 1 June 2010
Available online 8 June 2010

Keywords:
Hydrothermal
Solvothermal
Nest-like sphere
Hollow sphere
Redox reaction
Electrochemical properties

ABSTRACT

Two kinds of different Co–S microspheres with novel structure are synthesized by liquid phase chemical method (hydrothermal method and solvothermal method), and their formation mechanisms are also constructed. The electrochemical properties as negative electrode for alkaline secondary batteries are first performed using LAND battery test instrument. Co–S nest-like spheres electrode displays high reversible discharge capacity of 250 mAh g^{-1} and excellent cycle stability at current density 200 mA g^{-1}. The discharge curve and CV curve confirm that the reaction occurring on Co–S alloy electrode is a reversible redox reaction of Co. The higher specific surface areas of Co–S nest-like spheres may be responsible for the higher discharge capacity.

1. Introduction

Transition metal sulfides are of great interest for their excellent electronic, optical and mechanical properties and wide applications including solid lubricants, catalysts, lithium battery cathodes, thermal battery electrode, supercapacitor electrode, hydrogen storage materials, scanning probes, photoconductors and shockwave resistance materials [1–11].

Among the variety of transition metal sulfides, cobalt monosulfide (CoS) is one of the most important transition metal sulfides with pronounced catalytic activities for hydrodesulfurization and hydrodearomatization [12] and interesting paramagnetic properties [13]. Conventionally, cobalt sulfide powders were prepared by traditional solid state method [14], but the high temperature could lead to a large particle size and an inhomogeneity. Recently, extensive attention has been focused on the hydrothermal and solvothermal synthesis of transition metal sulfides powders [15,16], largely because the reaction can proceed at a mild temperature, and the size, morphology, and phase homogeneity of the production can be well controlled. However, most of the previous work reported is about Co_9S_8 and CoS_2 phases of cobalt sulfides, only few papers reported the synthesis of cobalt monosulfide (CoS) [17,18].

Wang et al. have prepared Co–S composite by ball-milling method and found that the alloy electrode shows relatively high discharge capacity and good cycling stability. The discharge capacity is 300 mAh g^{-1} and the capacity retention rate (C_{100}/C_{max}) is 86% [19].

Recently, we have synthesized S–$Co(OH)_2$ composite, which displays excellent electrochemical properties. Meanwhile, we have proposed the effect and function mechanism of amorphous S on the electrochemical properties of $Co(OH)_2$ electrode. The reaction on $Co(OH)_2$ negative electrode is the faradaic reaction between β-$Co(OH)_2$ and metallic Co during the charge–discharge process, so this mechanism can also be used to explain the function mechanism of some other metalloids (such as S, Si, B, P, BN, Si_3N_4, Se, CNTs) on metallic Co electrode [20].

To the best of our knowledge, except for Co–S composite, there has been no report on using CoS as the negative material of alkaline secondary batteries.

In this paper, CoS microspheres with novel structure are synthesized by liquid phase chemical method (hydrothermal method and solvothermal method). The formation mechanism of the fascinating structure are constructed. In addition, the electrochemical properties as negative electrode materials for alkaline secondary batteries are measured.

* Corresponding author. Tel.: +86 22 23503639; fax: +86 22 23503639.
E-mail address: wangyj@nankai.edu.cn (Y. Wang).

0378-7753/$ – see front matter © 2010 Elsevier B.V. All rights reserved.
doi:10.1016/j.jpowsour.2010.06.001

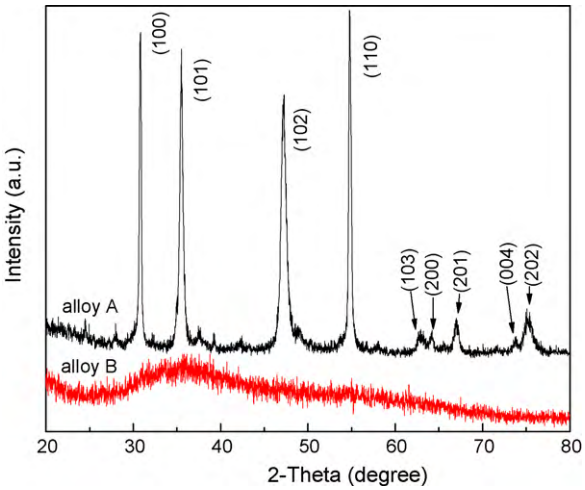

Fig. 1. XRD patterns of the Co–S samples.

2. Experiment

2.1. Preparation and structural characterization

$CoCl_2{\cdot}6H_2O$ and thiourea (Tu) were used as precursors for the preparation of Co–S microspheres. Sample A was prepared by hydrothermal method as follows: 1.5 g $CoCl_2{\cdot}6H_2O$ and 5.0 g thiourea were dissolved in 60 ml deionized water under stirring. Next, the precursor solution was transferred into Teflon-lined stainless steel autoclave, then the first hydrothermal treatment was carried out at 105 °C for 4 h, followed by the second hydrothermal treatment at 240 °C for 12 h. After the reaction, the powder was collected and washed with deionized water and finally vacuum-dried. Sample B was synthesized by solvothermal method in ethylene glycol (EG) solvent, and the preparation process was the same as sample A.

The elemental composition of the sample was measured by inductive coupled plasma atomic emission spectroscopy (ICP-AES) on a USA Themo Jarrel-Ash Corp. The crystal structure and morphology were characterized by X-ray diffraction (XRD, Rigaku D/Max-2500, Cu Kα radiation) and scanning electron microscopy (SEM, Hitachi X-650).

2.2. Electrochemical measurements

Negative electrodes were constructed as described previously [21]. Electrochemical measurements were conducted in a three compartment cell with a $NiOOH/Ni(OH)_2$ counter electrode and a Hg/HgO reference electrode using a Land battery test instrument. The electrolyte solution was a 6 M KOH aqueous solution. Charge–discharge cycle tests were performed by LAND battery test instrument (CT2001A). The electrodes were charged at 200 mA g^{-1}

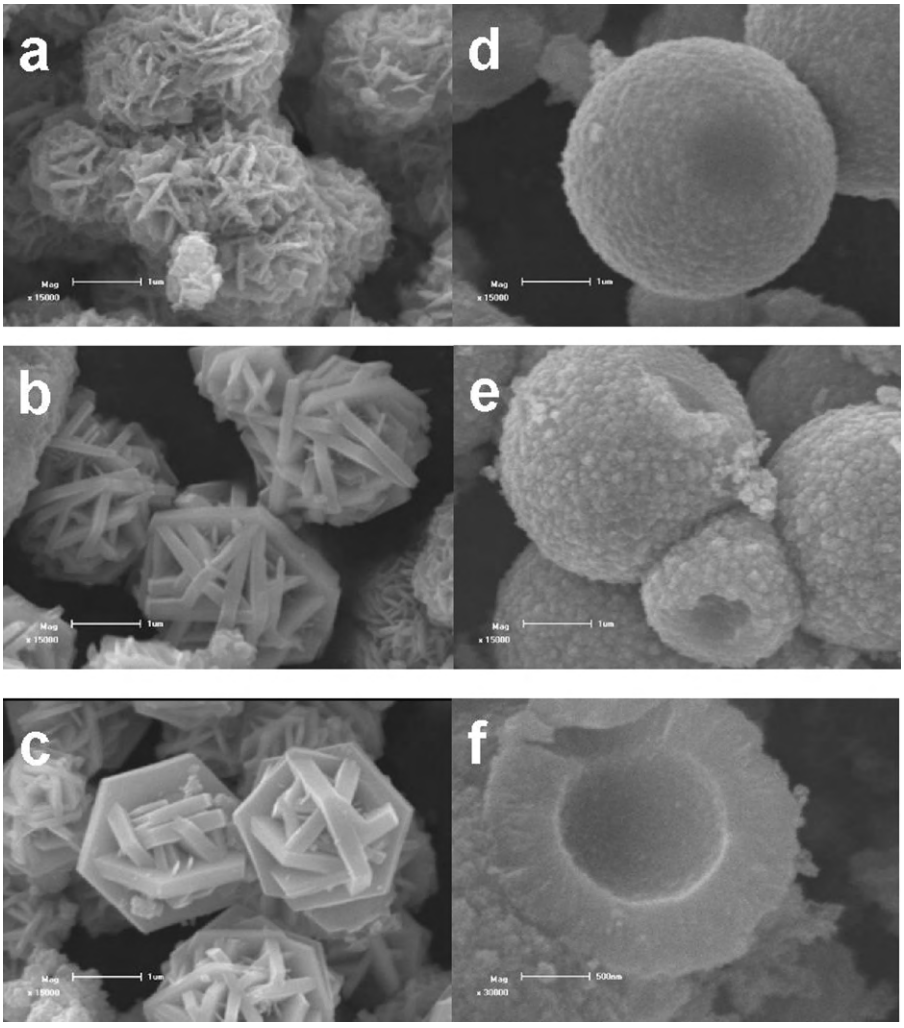

Fig. 2. SEM images of sample A (a: 160 °C, b: 200 °C, c: 240 °C) and sample B (d: 160 °C, e: 200 °C, f: 240 °C).

$$Tu + Co^{2+} \rightarrow Co(II)\text{-}Tu\ complex \xrightarrow{160^{\circ}C} Co\text{-}S\ flower\text{-}like spheres \xrightarrow{200^{\circ}C} Co\text{-}S\ nest\text{-}like spheres$$

Scheme 1. Schematic representation of the formation mechanism of Co–S nest-like spheres (alloy A).

for 3 h, discharged at 200 mA g^{-1} to −0.5 V vs. Hg/HgO, the interval between charge and discharge was 5 min.

3. Results and discussions

3.1. Material characterization

The XRD patterns of the Co–S samples are shown in Fig. 1. All peaks of sample A can be indexed to the hexagonal CoS (space group *P*63/*mmc*, JCPDS card No. 65-3418). The strong and sharp diffraction peaks indicate that sample A is well-crystalline. Moreover, no impurity peaks of other phases are detected, indicating the high purity of sample A. The ICP-AES is used to further determine the elemental composition of sample A, and the result shows that the atomic ratio of Co:S is also approximately about 1:1, corresponding well with the XRD pattern. Different from sample A, sample B shows a typical amorphous structure, as indicated by a weak broad peak located at $2\theta = 35^{\circ}$ with the width of 20°, and the atomic ratio of Co:S is approximately about 1:1.1.

The Co–S microspheres synthesized by two different methods display two different novel structures: sample A displays nest-like sphere structure which consists of some hexagonal disks (Fig. 2c), the edge of which is about 1.5 μm. Sample B displays hollow sphere structure (Fig. 2f) with the outer diameter of about 4.5 μm and inner diameter of 2.5 μm.

3.2. Formation mechanism

A fundamental understanding of the formation mechanism of novel structure Co–S microspheres is critical for achieving control over their properties. SEM images of Co–S microspheres obtained at different temperatures of the second step hydrothermal treatment are performed to investigate the formation mechanism (Fig. 2).

From the SEM images, Co–S flower-like spheres are observed at 160 °C (Fig. 2a). At 200 °C, flower-like spheres turn to nest-like spheres containing some hexagonal disks (Fig. 2b). At 240 °C, the structure of nest-like spheres becomes more simple and obvious (Fig. 2c).

From the above observation, the formation mechanism of Co–S nest-like spheres is assumed as follows: First, under the first hydrothermal treatment, the complexation Co(II)–Tu is formed in the mixed solution without the decomposition of Tu. Then at the second hydrothermal treatment, Co(II)–Tu complex decomposes to Co–S flower-like spheres and further decomposes to Co–S nest-like spheres, and the obtained hexagonal disks are attributed to the hexagonal system of sample A. In this process, Co(II)–Tu complex serves as not only intermediate but also self-template. The process is described in Scheme 1.

As to the formation process of sample B, round spheres with small nanocrystals coated are observed at 160 °C, and a place with dark color on the surface indicates that this place is thinner than other places (Fig. 2d). At 200 °C, round spheres turn into broken hollow spheres (Fig. 2e). At 240 °C, broken hollow spheres grow larger than those collected at 200 °C and further broke into hemispheres, showing that the diameter of hollow space is about 2.5 μm (Fig. 2f).

On the basis of the above observation, according to the formation mechanism of CuS hollow spheres and ZnO hollow spheres [22,23], the formation of Co–S hollow spheres can be explained by a bubble template mechanism. As illustrated in Scheme 2, in

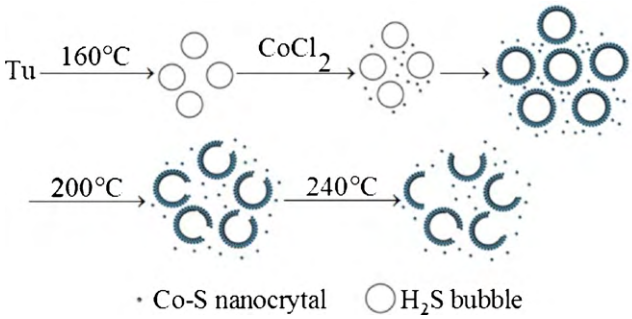

Scheme 2. Schematic representation of the formation mechanism of Co–S hollow spheres (alloy B).

EG solvent at 160 °C, Tu decomposes to H_2S bubbles, which react with $CoCl_2$ to form Co–S nanocrystals. These nanocrystals have a tendency to aggregate due to their high surface energies. Driven by the minimization of interfacial energy, small Co–S nanocrystals may aggregate around the gas–liquid interface between bubble and solvent and finally Co–S hollow spheres form. With the temperature increasing, the inside pressure of hollow spheres increases, and some hollow spheres are broken. In this process, the aggregation around the gas–liquid interface is going on all the same, so the hemispheres seems larger than those obtained at 200 °C.

3.3. Electrochemical performance

Fig. 3 shows the cycle life of Co–S microspheres as negative electrodes at current density 200 mA g^{-1}. There are only three activation cycles in Co–S nest-like spheres (sample A) electrode charge–discharge cycles. The reversible discharge capacity is about 250 mAh g^{-1} and remains quite stable in 40 cycles. Compared with sample A, Co–S hollow spheres (sample B) electrode exhibits lower reversible discharge capacity of only about 90 mAh g^{-1}. The much higher specific surface areas of Co–S nest-like spheres (sample A) may be responsible for the higher discharge capacity than that of Co–S hollow spheres (sample B).

Alloy A electrode exhibits high reversible discharge capacity and good cycle stability in charge–discharge cycles, But whether the reversible discharge capacity is attributed to the electrochemical hydrogen storage of the Co–S electrode, or to the redox reaction of Co in the Co–S alloy electrode? Fig. 4 shows the discharge curve of alloy A electrode at a constant current of 200 mA g^{-1}. The poten-

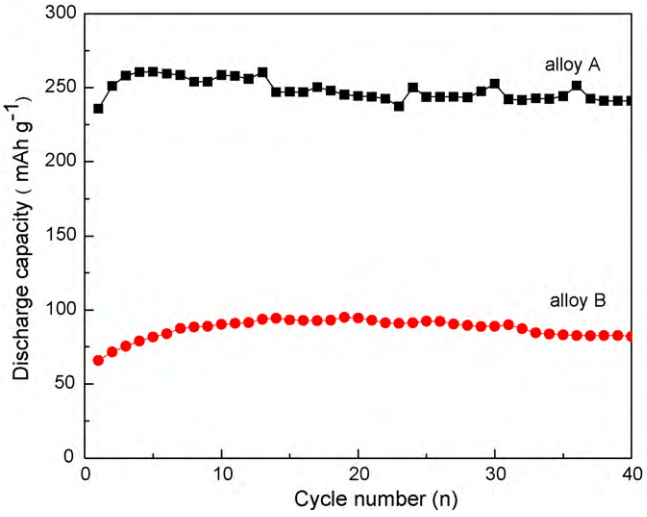

Fig. 3. Cycle life of alloy A and alloy B electrodes at a rate of 200 mA g^{-1}.

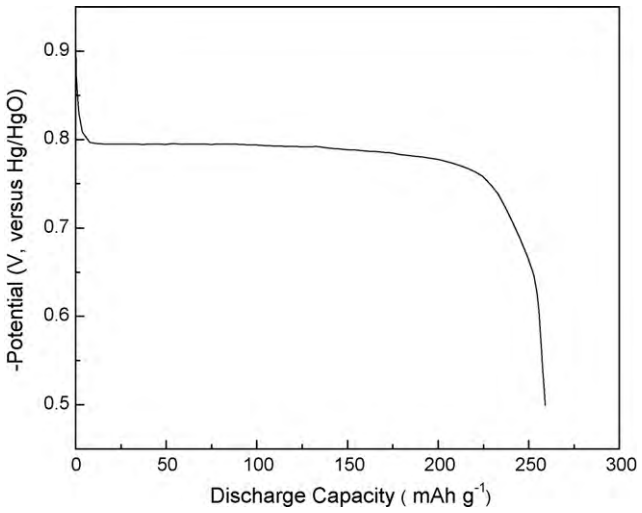

Fig. 4. Typical discharge curve of alloy A electrode at a current of 200 mA g^{-1}.

tial plateau appears at about −0.80 V (vs. Hg/HgO), very similar to the potential plateaus of Co–Si_3N_4 and Co-BN composite electrodes reported by Gao group [24,25]. It is known that the equilibrium potential of the Co/$Co(OH)_2$ couple corresponds to −0.83 to −0.85 V (vs. Hg/HgO) in a alkaline solution [26]. So the plateau potential, which shows a slight overpotential can be explained by the oxidation process of Co. To further confirm the electrochemical reaction process of Co–S alloy electrode, CV curve is presented in Fig. 5. It is observed that a pair of remarkable cathodic and anodic current peaks appear at −0.96 V (vs. Hg/HgO) and −0.47 V (vs. Hg/HgO), respectively, suggesting a reversible electrochemical oxidation-reduction process occurring on Co–S alloy electrode. Considering that the potential positions and shapes of these current peaks very well resembles that of Co in Co-BN composite electrode and it is reasonable to attribute the pair of the reduction–oxidation peaks to the redox reaction of Co on Co–S alloy electrode. Based on the above experimental results, it can be concluded that the reversible charge–discharge processes of Co–S alloy electrode proceed mainly through redox reaction of Co and the electrode reaction can be expressed as:

$$Co + 2OH^- \underset{\text{charge}}{\overset{\text{discharge}}{\rightleftarrows}} Co(OH)_2 + 2e \quad (1)$$

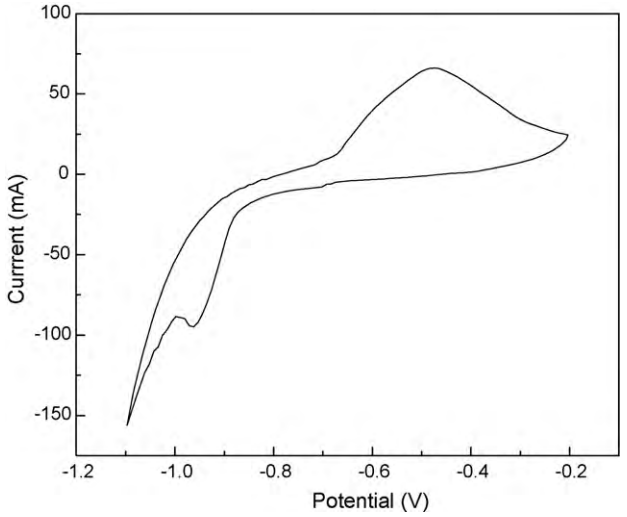

Fig. 5. CV curve of alloy A electrode at scan rate of 1 mV s^{-1}.

S in Co–S composite electrode shows two functions during the charge–discharge process. One is that the addition of S improves the dispersion of Co particles. The other is that the dissolution of S brings new interspaces among the Co particles. These two factors largely increase contact area of Co particles and alkaline solution, which is in favor of the surface electrochemical redox. Thus, the capacity utilization of Co is enhanced. Different from Co–S composite, Co–S alloy synthesized by liquid phase chemical method possess strong Co–S bond, which is difficult to be destroyed by the corrosion of alkaline solution, leading to less new interspaces among the Co particles. So the capacity utilization of Co is low and the practical capacity is ca. 250 mAh g^{-1}, lower than that of Co–S composite electrode.

4. Conclusion

In summary, Co–S nest-like spheres of hexagonal CoS phase and Co–S hollow spheres of amorphous structure are synthesized by hydrothermal method and solvothermal method, respectively, and their formation mechanism are also constructed. They are first investigated as negative electrode materials for alkaline secondary batteries, showing that the Co–S nest-like spheres electrode has higher capacity and cycle stability than Co–S hollow spheres electrode. The discharge curve and CV curve confirmed the reaction occurring on Co–S alloy electrode was a reversible redox reaction of Co. Further detailed investigations on Co–S alloy are now in progress.

Acknowledgments

This work is financially supported by MOST program (2007AA05Z149, 2007AA05Z108, 2010CB631303), NSFC (50631020, 50701025, 50971071).

References

[1] R. Tenne, L. Margulis, M. Genut, G. Hodes, Nature 360 (1992) 444–446.
[2] R. Tenne, Angew. Chem. Int. Ed. 42 (2003) 5124–5132.
[3] P.G. Li, M. Lei, X.F. Wang, H.L. Tang, W.H. Tang, J. Alloys Compd. 474 (2008) 463–467.
[4] M. Lei, H. Yang, P.G. Li, W.H. Tang, Appl. Surf. Sci. 254 (2008) 1947–1952.
[5] V. Petkov, S.J.L. Billinge, J. Heising, M.G. Kanatzidis, J. Am. Chem. Soc. 122 (2000) 11571–11576.
[6] J. Heising, M.G. Kanatzidis, J. Am. Chem. Soc. 121 (1999) 11720–11732.
[7] M. Remskar, A. Mrzel, Z. Skraba, A. Jesih, M. Ceh, J. Demsar, P. Stadelmann, F. Levy, D. Mihailovic, Science 292 (2001) 479–481.
[8] A. Rothschild, J. Sloan, R. Tenne, J. Am. Chem. Soc. 122 (2000) 5169–5179.
[9] P. Butler, C. Wagner, R. Guidotti, I. Francis, J. Power Sources 136 (2004) 240–245.
[10] F. Tao, Y.Q. Zhao, G.Q. Zhang, H.L. Li, Electrochem. Commun. 9 (2007) 1282–1287.
[11] J. Chen, N. Kuriyama, H.T. Yuan, H.T. Takeshita, T. Sakai, J. Am. Chem. Soc. 123 (2001) 11813–11814.
[12] Y.E. Hiraka, J. Phys. Soc. Jpn. 63 (1994) 4573–4575.
[13] D. Hobbs, J. Hafner, J. Phys.: Condens. Matter. 11 (1999) 8197–8199.
[14] A. Wold, K. Dwight, J. Solid State Chem. 96 (1992) 53–58.
[15] X.F. Qian, Y.D. Li, Y. Xie, Y.T. Qian, Mater. Chem. Phys. 66 (2000) 97–99.
[16] J.H. Zhan, X.G. Yang, Y. Xie, D.W. Wang, Y.T. Qian, X.M. Liu, J. Mater. Res. 14 (1999) 4418–4420.
[17] X.C. Sun, K. Parvin, J. Ly, D.E. Nikles, IEEE Trans. Magn. 39 (2003) 2678–2680.
[18] J.H. Zhan, Y. Xie, X.G. Wang, W.X. Zhang, Y.T. Qian, J. Solid State Chem. 146 (1999) 36–38.
[19] Q.H. Wang, L.F. Jiao, H.M. Du, W.X. Peng, S.C. Liu, Y.J. Wang, et al., Int. J. Hydrogen Energy (2010), doi:10.1016/j.ijhydene.2009.12.002.
[20] D.W. Song, Y.J. Wang, Q.H. Wang, Y.P. Wang, L.F. Jiao, H.T. Yuan, J. Power Sources (2010), doi:10.1016/j.jpowsour.2010.04.088.
[21] D.W. Song, Y.J. Wang, Y.P. Wang, L.F. Jiao, H.T. Yuan, Electrochem. Commun. 10 (2008) 1486–1489.
[22] J. Liu, D.F. Xue, J. Cryst. Growth 311 (2009) 500–503.
[23] C.L. Yan, D.F. Xue, J. Alloys Compd. 431 (2007) 241–245.
[24] S.M. Yao, K. Xi, G.R. Li, X.P. Gao, J. Power Sources 184 (2008) 657–662.
[25] Z.W. Lu, S.M. Yao, G.R. Li, T.Y. Yan, X.P. Gao, Electrochim. Acta 53 (2008) 2369–2375.
[26] Y.L. Cao, W.C. Zhou, X.Y. Li, X.P. Ai, X.P. Gao, H.X. Yang, Electrochim. Acta 51 (2006) 4285–4290.